Neutron Time-of-Flight Measurements of Charged-Particle Energy Loss in Inertial Confinement Fusion Plasmas

D. B. Sayre,[1,*] C. J. Cerjan,[1,†] S. M. Sepke,[1] D. O. Gericke,[2] J. A. Caggiano,[1] L. Divol,[1] M. J. Eckart,[1] F. R. Graziani,[1] G. P. Grim,[1] S. B. Hansen,[3] E. P. Hartouni,[1] R. Hatarik,[1] S. P. Hatchett,[1] A. K. Hayes,[4] L. F. Berzak Hopkins,[1] M. Gatu Johnson,[5] S. F. Khan,[1] J. P. Knauer,[6] S. LePape,[1] A. J. MacKinnon,[1] J. M. McNaney,[1] N. B. Meezan,[1] H. G. Rinderknecht,[1] D. A. Shaughnessy,[1] W. Stoeffl,[1] C. B. Yeamans,[1] A. B. Zylstra,[4] and D. H. Schneider[1]

[1] *Lawrence Livermore National Laboratory, Livermore, California 94550, USA*
[2] *Centre for Fusion, Space and Astrophysics, Department of Physics, University of Warwick, Coventry CV4 7AL, United Kingdom*
[3] *Sandia National Laboratory, Albuquerque, New Mexico 87185, USA*
[4] *Los Alamos National Laboratory, Los Alamos, New Mexico 87545, USA*
[5] *Massachusetts Institute of Technology, Cambridge, Massachusetts 02139, USA*
[6] *University of Rochester, Rochester, New York 14623, USA*

(Dated: January 8, 2020)

Neutron spectra from secondary $^3\mathrm{H}(d,n)\alpha$ reactions produced by an implosion of a deuterium-gas capsule at the National Ignition Facility have been measured with order-of-magnitude improvements in statistics and resolution over past experiments. These new data and their sensitivity to the energy loss of fast tritons emitted from thermal $^2\mathrm{H}(d,p)^3\mathrm{H}$ reactions enable the first statistically significant investigation of charged-particle stopping via the emitted neutron spectrum. Radiation-hydrodynamic simulations, constrained to match a number of observables from the implosion, were used to predict the neutron spectra while employing two different energy loss models. This analysis represents the first test of stopping models under inertial confinement fusion conditions, covering plasma temperatures of $k_BT \approx 1$–4 keV and particle densities of $n \approx 12$–2×10^{24} cm^{-3}. Under these conditions, we find significant deviations of our data from a theory employing classical collisions whereas the theory including quantum diffraction agrees with our data within error bars.

PACS numbers: 52.57.-z,34.50.Bw,29.30.-h

Understanding the rate that energetic ions ($E \gg k_BT$) deposit energy along their paths through dense plasmas is fundamental to inertial confinement fusion research, as it strongly constrains the hot core conditions required to ignite the deuterium-tritium fuel. Reports of recent implosions [1–4] with layered deuterium-tritium capsules [5] attribute a significant part of the measured neutron yield from $^3\mathrm{H}(d,n)\alpha$ reactions to plasma heating by the associated α-particles. Surrogate experiments with pure deuterium-gas targets [6–9] use yields from reactions with energetic charged-particles to infer plasma conditions, such as areal density and electron temperature [10–12] or capsule-fuel mixing [13]. Results derived from both types of experiments depend on assumptions for the stopping power of hydrogen plasmas at temperatures of $k_BT \approx 1$–4 keV and corresponding densities of $\rho \approx 100$–10 g/cm^3 [14]. Moreover, while energy loss models exist for these hot, dense plasmas [15–18], measurements to verify their predictions under these conditions remain a challenge.

Several experiments [19, 20] have been conducted with capsules containing mixtures of deuterium and helium-3 to measure the energy downshift of fast hydrogen and helium ions that emerge from thermal reactions within hot (≈ 0.5–13 keV) plasmas at lower densities ($\lesssim 10^{23}$ cm^{-3}). When the plasma dimensions do not exceed the ion ranges and energy loss due to ablator material [21] is negligible, this direct method has been used to evaluate the fuel's stopping power under weakly coupled and non-degenerate conditions [20].

The extension of this investigation to denser plasmas similar to the thermonuclear cores of layered deuterium-tritium experiments, in which neither criteron may be satisfied, motivates indirect approaches to detect charged-particle energy loss. In particular, the neutron spectrum [22] emitted by $^3\mathrm{H}(d,n)\alpha$ reactions within an imploded deuterium-gas capsule has been identified [12] as a way to study the stopping of fast tritons in denser plasmas [23].

Recent progress made on implosions with deuterium-gas capsules at the National Ignition Facility [24, 25] has led to orders of magnitude higher secondary $^3\mathrm{H}(d,n)\alpha$ yields than previous experiments [26] and enabled time-of-flight spectroscopy with similar gains in precision. *In this Letter*, we apply this new capability to the approach proposed nearly three decades ago by Cable & Hatchett [12] and report the first statistically significant investigation of charged-particle energy loss with the neutron spectrum.

Thermal $^2\mathrm{H}(d,p)^3\mathrm{H}$ reactions within the hot core formed by imploding a deuterium-gas capsule create an isotropic and nearly monoenergetic source of tritons with approximately 1.01 MeV. A small fraction (10^{-2}) of these

tritons initiate $^3\mathrm{H}(d,n)\alpha$ reactions before either thermalizing or exiting the hot core plasma. For comparison, the neutron yields from secondary $^3\mathrm{H}(d,n)\alpha$ reactions are a factor of 10^4 lower than those from the thermal reactions in deuterium-tritium implosions. The signal of secondary neutrons is further reduced by the inefficiencies of the time-of-flight measurements (detector at 20 m distance) required to measure the spectrum with a resolution of $\delta E/E \approx 2\%$ over the range of 12–17 MeV. So far these harsh requirements have not been met (see Ref. [7] for the only attempt to investigate energy loss through the neutron spectrum).

The secondary $^3\mathrm{H}(d,n)\alpha$ neutron spectrum observed from an implosion reflects the velocities of interacting tritons in addition to the known angular distribution of the neutrons. The two-body kinematics of the reaction transform these velocities into the spectrum. The energy loss in the plasma modifies the magnitude of the triton's velocities and, thus, affects the distribution of reaction energies. Changes in the triton energy are magnified by the energy dependence of the $^3\mathrm{H}(d,n)\alpha$ cross section [27]. In total, the reaction probability is inversely proportional to the stopping power [28].

The conditions of the hydrogen plasma, together with the triton's energy, determine the stopping power. Fig. 1 illustrates the plasma conditions determined by radiation-hydrodynamic simulation [29]. The simulations were constrained to match the time of the peak x-ray emission, the total neutron yield and the spectral widths of the neutron emission (similar as in Ref. [24]). These quantities are quoted in table I for both the simulations and as observed in our experiment (N130813).

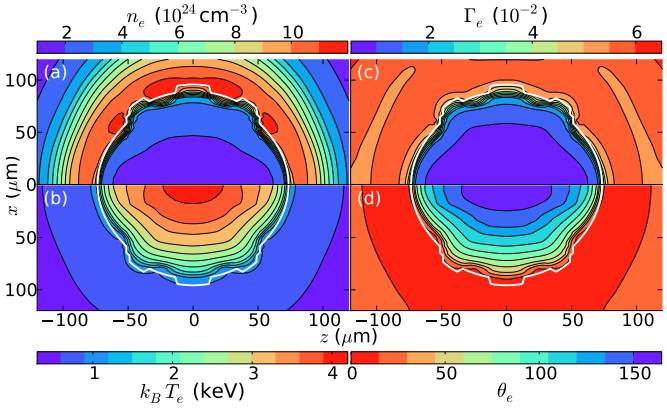

FIG. 1. (color online) Results of two-dimensional HYDRA [29] simulations, symmetric about the z-axis (hohlraum axis) for (a) the electron density n_e, (b) the temperature $k_b T_e$, (c) the electron coupling Γ_e, and (d) electron degeneracy θ_e at peak energy production in experiment N130813. The white curve defines the boundary between the fuel and surrounding carbon ablator. The observed $^3\mathrm{H}(d,n)\alpha$ neutron spectrum is sensitive only to the weakly coupled, nondegenerate plasma inside the white curve.

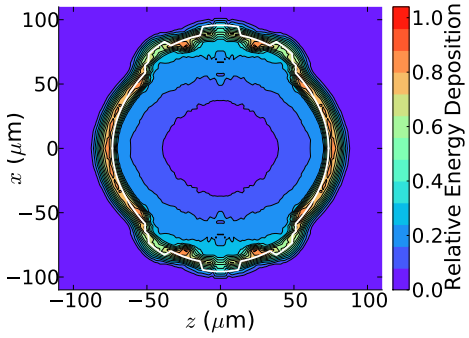

FIG. 2. (color online) Map of the energy deposition of tritons in the plasma, summed over the burn duration and weighted by volume. The highest energy deposition occurs in the low-temperature, high-density regions surrounding the hot core. Tritons that escape the deuterium plasma are quickly stopped in the remaining carbon ablator (outside the white curve).

The relevant region in our experiment is the hot core of the implosion with temperatures of $k_B T = 1$–4 keV and relatively moderate densities of 12–2×10^{24} cm^{-3}. Fig. 2 displays the energy deposited by tritons as they traversed the plasma using the plasma conditions from the HYDRA simulation. Within a single implosion, we examine the stopping power of the deuterium plasma integrated over conditions in the core region by comparing the neutron spectra measured with two time-of-flight detectors with those obtained by the simulations. For comparison, we can switch between two commonly employed energy loss models [15, 16] in the simulation.

Figure 3 illustrates how the interacting tritons and the corresponding neutron spectrum respond to the plasma conditions as shown in Fig. 1. Our conditions overlap with the parameters of hot cores of layered deuterium-tritium implosions, and afford the first comparison of stopping models with experimental data directly relevant to inertial confinement fusion.

To calculate the $^3\mathrm{H}(d,n)\alpha$ neutron spectrum requires simulating the production and transport of tritons, from their origins in the hot core to their interaction points throughout the plasma. Of course, this simulation must also describe the plasma's spatiotemperal evolution over the thermonuclear stage of the implosion as it modifies both processes. The standard prescription in HYDRA for the charged-particle energy loss within the fully ionized, hot hydrogen plasmas uses Maynard and Deutsch's [15] version of the random phase approximation for electron stopping and a binary collision description for ions [30]. For comparison, we include another model frequently used to calculate electron stopping power under these conditions: the Fokker-Planck formulation given by Li and Petrasso [16].

The experiments analysed employ spherical capsules filled with pure deuterium gas. A set of capsules was ablatively imploded using the indirect drive technique

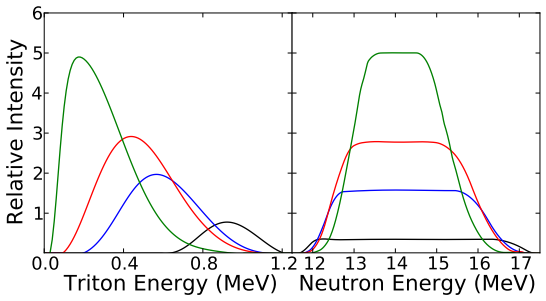

FIG. 3. (color online) Energy distributions of reacting tritons (left panel) and their associated neutron spectra (right panel) as simulated using the plasma conditions shown in Fig. 1 and the default stopping model in HYDRA [30] for a set of radii spanning the deuterium plasma: 10–20 μm (black), 60–70 μm (blue), 70–80 μm (red), and from 80 μm to the carbon ablator (green). The mean triton energy decreases with radius, which reduces the Doppler shift and, thus, narrows the distribution of emitted neutrons. The energy loss also strongly increases the relative intensity of the neutron spectrum as the tritons approach the strong resonance in the ^{3}H$(d,n)\alpha$ cross section at a triton energy of 160 keV. An analogous behavior occurs in time: as the plasma cools and becomes more dense during the thermonuclear burn duration, the spectrum narrows and the ^{3}H$(d,n)\alpha$ yield per triton increases.

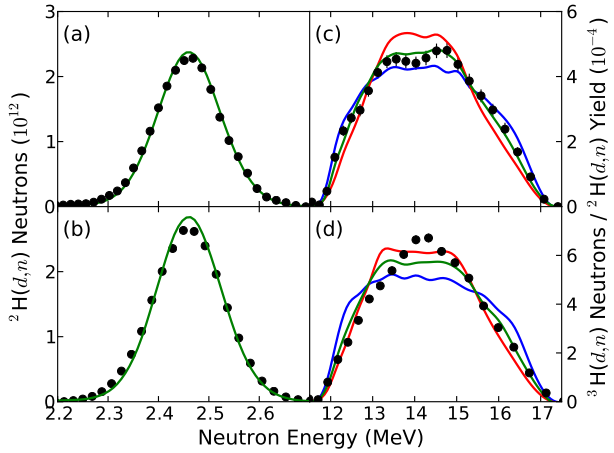

FIG. 4. (color online) Spectra of ^{2}H$(d,n)^3$He and ^{3}H$(d,n)\alpha$ reactions extracted from detectors (•) along the lines of sight $(\theta,\phi) = (115°, 316°)$ in panels (a) and (c), and $(161°, 56°)$ in panels (b) and (d). The data points are spaced in increments of the full width at half maximum of each detector's impulse response function, and contain statistical uncertainties (which are smaller than the marker size) from neutron interactions, photoelectrons, and digitizer noise. Simulated spectra (lines) are normalized to the measurements to emphasize differences in shapes. Results for the Maynard and Deutsch [15] (red) and Li and Petrasso [16] (blue) stopping power models are shown for ^{3}H$(d,n)\alpha$ spectra; only Maynard and Deutsch is shown for the ^{2}H$(d,n)^3$He spectra as they are independent of stopping model. Note that a higher degree of asymmetry in areal density and/or plasma conditions than was accounted for in the simulations is believed to be responsible for the bad agreement shown in panel (d) [39].

at the National Ignition Facility [31] as part of an experimental campaign assessing the performance of high-density carbon ablators [24]. These implosions were of particular interest due to their reported high symmetry and absence of observed capsule-fuel mixing. From this set of experiments, we focus here on the implosion that produced the highest yields (N130813). Here, the ^{2}H$(d,n)^3$He and ^{3}H$(d,n)\alpha$ yields were in excess of 10^{13} and 10^{11}, respectively [9, 24].

Two time-of-flight spectrometers [32] with bibenzyl scintillators [33] provided current mode measurements of neutron events at distances of 18 and 22 m from the target, along the $(\theta,\phi) = (161°, 56°)$ and $(115°, 316°)$ lines of sight, respectively. Each spectrometer collected ^{3}H$(d,n)\alpha$ and ^{2}H$(d,n)^3$He data from the implosion using four photodetectors to assure signal quality. The events due to both reactions generated signals with statistical precisions better than 1% [34], where the signals from the reactions contained no observable background. The downscattering of neutrons by compressed material of the capsule was observed to have little effect on the ^{3}H$(d,n)\alpha$ and ^{2}H$(d,n)^3$He signals [35].

The ^{2}H$(d,n)^3$He signal contains several important pieces of information for the present investigation. The yield of the ^{2}H$(d,n)^3$He neutron peak determines how many tritons were emitted from ^{2}H$(d,p)^3$H reactions, as deuterium fusion proceeds equally through both channels for the temperatures created by the implosion [36]. Thus, the yield combined with the observed peak broadening are a diagnostic of hot core conditions. General aspects of the ^{2}H$(d,n)^3$He analysis are discussed in Ref. [37].

To perform the analysis of the secondary reaction, ^{3}H$(d,n)\alpha$, the related neutron energy spectrum must be extracted from the digitized photodetector signals to correct for scintillator response and neutron transmission through materials in the line of sight [38]. First, the raw signals are aligned to a timing fiducial indicating peak x-ray production from the implosion. In the next step, a fitting algorithm, which parametrizes the spectrum with a penalized spline [37], separates the measured impulse response functions of the detection systems. In Fig. 4, the resulting spectrum for each detector is displayed. Note that, if tritons did not lose energy, the measured ^{3}H$(d,n)\alpha$ spectra would have a flat distribution due to the reaction's isotropy [12].

Activation foil measurements [40] were employed to calibrate the yields of fitted ^{3}H$(d,n)\alpha$ and ^{2}H$(d,n)^3$He spectra resulting in systematic uncertainties of 8%. The ratio of ^{3}H$(d,n)\alpha$ to ^{2}H$(d,n)^3$He yields from both spectrometers determines that $(7.0\pm0.8)\times10^{-3}$ of the tritons created react in the present experiment. Uncertainties from each yield are summed in quadrature to give the ratio's uncertainty of 11%.

We perform an integrated analysis of the observables

TABLE I. Comparison of the metrics from the simulation and diagnostic measurements for experiment N130813.

Observable	Measurement (θ, ϕ)		HYDRA (θ, ϕ^{a})	
	$(115, 316)$	$(161, 56)$	$(115, 316)$	$(161, 56)$
^{2}H(d,n) yield (10^{13})	2.2 ± 0.2	2.2 ± 0.2	2.0[b]	2.0[b]
^{3}H(d,n) yield (10^{11})	1.5 ± 0.1	1.6 ± 0.1	1.6[c]	1.6[c]
			1.9[d]	1.9[d]
Yield ratio (10^{-3})	7.0 ± 0.8	7.0 ± 0.8	8.0[c]	8.0[c]
			9.3[d]	9.3[d]
^{2}H(d,n) *std.*[e](keV)	69 ± 3	71 ± 3	66	68
Bang time[f] (ns)	7.86 ± 0.02		7.68	
Burn width[g] (ps)	290 ± 20		310	

[a] 2D HYDRA simulations are azimuthally symmetric.
[b] Independent of stopping power model.
[c] Maynard and Deutsch stopping power model.
[d] Li and Petrasso stopping power model.
[e] Standard deviation calculated from fit over 2.2–2.7 MeV.
[f] Peak x-ray emission [41].
[g] Full width at half maximum of x-ray emission [41].

from experiment N130813 using two-dimensional HYDRA simulation to model the plasma conditions and neutron spectrum [42, 43]. Table I summarizes the agreement between the simulations and present experiment. It also highlights the predicted differences in the ^{3}H$(d,n)\alpha$ yield related to the different stopping models applied to slow down the tritons in the plasma.

The difference between simulated results for the two stopping models is measurable within the accuracy of the ^{3}H$(d,n)\alpha$ spectrum, both by its integral and its shape. The ratios of ^{3}H$(d,n)\alpha$ to ^{2}H$(d,n)^{3}$He yields listed in Table I show Li and Petrasso's model gives a 32% larger value than the experiment, while the one for Maynard and Deutsch's model is high by 13%, just slightly above the measurement uncertainty of 11%. The theoretical predictions differ by roughly two standard deviations of the measurements allowing for a distinction between the models. Our experimental data strongly favor Maynard and Deutsch's theory for the hot spot conditions, as the ^{3}H$(d,n)\alpha$ yield predicted with the Li and Petrasso model exceeds the measurements by more than three standard deviations.

The predictions from the two stopping models tested differ so strongly because most reactions occur in the dense fuel near the boundary of the hot spot and the ablator (see Fig. 2). Before they reach this region, most triton have traveled a longer path through the plasma and the differences between stopping models accumulate over that path. The deviations are further amplified by the strong resonance in the cross section for the ^{3}H$(d,n)\alpha$ fusion reaction. By predicting a larger energy loss, the Li and Petrasso model increases the overlap between the triton's energy distribution and the resonance. Although the reaction probability also has an inverse relationship with the stopping power as a larger energy loss results in less areal density at each triton energy, the yield, in this case, is dominated by the degree of overlap with the resonance.

The differences between the stopping models can also be observed in the shape of the neutron spectra. The extra reactions predicted by the Li and Petrasso model occur mainly at lower triton energies, thus, populating the neutron spectrum at energies of 13–15 MeV. This contribution makes the area-normalized spectra appear more narrow for the Li and Petrasso model than it is predicted with the Maynard and Deutsch approach (see Figs. 4 (c) and (d)). A χ^2_ν analysis of the spectra gives values of 1.1 (top, $\nu = 24$) and 11.1 (bottom, $\nu = 20$) for the Maynard and Deutsch and 3.6 (top) and 11.2 (bottom) for Li and Petrasso models which quantifies the better match by the approach of Maynard and Deutsch related to the shape of the neutron spectrum.

The physical reasons for the observed differences in stopping models may be found in the different treatment of collisions. Whereas the Li and Petrasso model has classical collisions at its basis, the approach of Maynard and Deutsch is equivalent to the full quantum treatment within RPA [44]. However, it is not quantum degeneracy that drives the differences as indicated by the large value of Θ; instead, quantum diffraction significantly modifies the cross section of triton-electron collisions at the high plasma temperatures considered here.

The effect of quantum diffraction can be quantified by the Born parameter $\xi = \varrho/\lambda_{dB}$ which is the ratio of the distance of closest approach and the electron deBroglie wavelength. For the conditions in the hot core, we find $0.08 < \xi < 0.1$, that is, the deBroglie wavelength is far larger than the interaction zone requesting a quantum description of scattering. Neglecting quantum diffraction strongly degrades the performance of the Li and Petrasso model for our conditions. The small deviations of the RPA-like model and the measurements might be related to the neglect of strong scattering [44] which is of minor importance for the conditions in the core of the implosion but has been recently observed more clearly for particle velocities around the Bragg peak [45, 46].

In conclusion, the order-of-magnitude improvement in neutron spectroscopy of secondary ^{3}H$(d,n)\alpha$ reactions at the National Ignition Facility enable investigations of charged-particle energy loss using these neutron spectra. This method extends studies of stopping power to hot, dense plasmas directly relevant to inertial confinement fusion. Here, an improved understanding of self-heating by α-particle is necessary to evaluate the performance of experiments and guide future designs. Our data are accurate enough to distinguish between the models of Li and Petrasso and the RPA-like approach by Maynard and Deutsch. Whereas the latter is roughly consistent with our measured neutron spectra, the prediction of the Li and Petrasso model are three standard deviations away from the data. These differences may be attributed to

the incorporation or neglect of quantum diffraction in the underlying scattering theory of these stopping models.

We thank O. L. Landen for useful discussions and also express our appreciation to the operations staff at the National Ignition Facility for making the investigation possible. This work was performed under the auspices of Lawrence Livermore National Security, LLC, Contract No. DE-AC52-07NA27344.

* sayre4@llnl.gov
† cerjan1@llnl.gov

[1] O. A. Hurricane *et al.*, Nature **506**, 343 (2014).
[2] T. Döppner *et al.*, Phys. Rev. Lett. **115**, 055001 (2015).
[3] T. Ma *et al.*, Phys. Rev. Lett. **114**, 145004 (2015).
[4] S. Le Pape *et al.*, Phys. Rev. Lett. **120**, 245003 (2018).
[5] B. J. Koziokiemski *et al.*, Fusion Sci. Technol. **59**, 14 (2011).
[6] H. Azechi *et al.*, J. Appl. Phys. Lett. **49**, 555 (1986).
[7] M. D. Cable *et al.*, Phys. Rev. Lett. **73**, 2316 (1994), see neutron spectrum shown in Fig. 3.
[8] S. Kurebayashi *et al.*, Phys. Plasmas **12**, 032703 (2005).
[9] H. G. Rinderknecht *et al.*, Phys. Plasmas **22**, 082709 (2015).
[10] E. G. Gamalii, S. Y. Gus'Kov, O. N. Krokhin, and V. B. Rusanov, JETP Lett. **21**, 70 (1975).
[11] T. E. Blue and D. B. Harris, Nucl. Sci. Eng. **77**, 463 (1981).
[12] M. D. Cable and S. P. Hatchett, J. Appl. Phys. **62**, 2233 (1987).
[13] H. Azechi *et al.*, Phys. Rev. Lett. **59**, 2635 (1987).
[14] These are weakly coupled and nondegenerate conditions as indicated by coupling and degeneracy parameters of $\Gamma_e \approx (1-6)\times 10^{-2}$ and $\theta_e \approx 130-7$. The coupling parameter is defined by $\Gamma_e = e^2[a(k_BT + E_F)]^{-1}$ where a is the Wigner-Seitz radius and E_F is the Fermi energy; the degeneracy parameter is given by $\theta_e = k_BT/E_F$.
[15] G. Maynard and C. Deutsch, J. Physique **46**, 1113 (1985).
[16] C. K. Li and R. D. Petrasso, Phys. Rev. Lett. **70**, 3059 (1993); Erratum, *ibid.* **114**, 199901 (2015).
[17] D. O. Gericke and M. Schlanges, Phys. Rev. E **60**, 904 (1999).
[18] L. S. Brown, D. L. Preston, and R. L. Singleton, Phys. Rep. **410**, 237 (2005).
[19] D. G. Hicks *et al.*, Phys. Plasmas **7**, 5106 (2000).
[20] J. A. Frenje *et al.*, Phys. Rev. Lett. **115**, 205001 (2015).
[21] In inertial confinement fusion experiments the fuel is compressed by ablating a surrounding shell of material.
[22] Neutral particles also avoid spectral distortions due to the strong electromagnetic fields generated by laser-plasma interactions outside the capsule.
[23] We also note the (energy integrated) neutron activation measurements of Ref. [47] used to investigate stopping models for strongly coupled, degenerate fuel conditions.
[24] A. J. Mackinnon *et al.*, Phys. Plasmas **21**, 056318 (2014).
[25] J. S. Ross *et al.*, Phys. Rev. E **91**, 021101(R) (2015).
[26] The secondary $^3\mathrm{H}(d,n)\alpha$ yield in the present experiment is $(1.6\pm0.1)\times10^{11}$ [9], while other experiments reported yields of 10^6 [6], 10^8 [7, 8, 48], and 10^{10} [49].
[27] The cross section of $^3\mathrm{H}(d,n)\alpha$ reactions is understood both theoretically and experimentally to a few percent [36], and does not complicate this analysis.
[28] The probability P that an energetic triton undergoes a $^3\mathrm{H}(d,n)\alpha$ reaction can be expressed as an integral over its energy in the deuterium plasma, $P = \int \frac{n\sigma(E)}{dE/dx(E)}dE$, in which the density of deuterium is n, the cross section is σ, and the stopping power is dE/dx.
[29] M. M. Marinak, G. D. Kerbel, N. A. Gentile, O. Jones, D. Munro, S. Pollaine, T. R. Dittrich, and S. W. Haan, Phys. Plasmas **8**, 2275 (2001).
[30] S. Sepke, Lawrence Livermore National Laboratory Report No. LLNL-TR-654859 (2014).
[31] J. Lindl, Phys. Plasmas **2**, 3933 (1995).
[32] T. J. Clancy *et al.*, Proc. SPIE **9211A**, 9211 (2014).
[33] R. Hatarik *et al.*, Plasma Fusion Res. **9**, 4404104 (2014).
[34] The primary contribution to signal fluctuations comes from the number of neutron hits in the scintillator, which a total of 3×10^4 and 5×10^6 for the $^3\mathrm{H}(d,n)\alpha$ and $^2\mathrm{H}(d,n)^3\mathrm{He}$ reactions, respectively.
[35] Only 3% of $^3\mathrm{H}(d,n)\alpha$ neutrons and 6% of $^2\mathrm{H}(d,n)^3\mathrm{He}$ neutron are expected to interact with capsule material.
[36] H.-F. Bosch and G. M. Hale, Nucl. Fusion **32**, 611 (1992).
[37] R. Hatarik *et al.*, J. Appl. Phys. **18**, 184502 (2015).
[38] Neutron attenuation from materials in the detector line of sights (port covers from the target chamber, either 1 cm of aluminum or 0.5 cm of steel, and x-ray filters which are 1 cm of tungsten) is accounted for with MCNP simulations.
[39] C. Cerjan, D. Sayre, and S. Sepke, Phys. Plasmas **25**, 022705 (2018).
[40] C. B. Yeamans, D. L. Bleuel, and L. A. Bernstein, Rev. Sci. Instrum. **83**, 10D315 (2012).
[41] S. F. Khan *et al.*, Proc. SPIE **8505**, 850505 (2012).
[42] C. J. Cerjan, (unpublished).
[43] S. V. Weber *et al.*, Phys. Plasmas **21**, 112706 (2014).
[44] D. O. Gericke, Laser Part. Beam **20**, 471 (2002).
[45] W. Cayzac *et al.*, Nat. Comm. **8**, 15693 (2017).
[46] J. A. Frenje *et al.*, Phys. Rev. Lett. **122**, 015002 (2019).
[47] A. Hayes *et al.*, Phys. Plasmas **22**, 082703 (2015).
[48] V. Y. Glebov *et al.*, Rev. Sci. Instrum. **72**, 824 (2001).
[49] P. F. Schmit *et al.*, Phys. Rev. Lett. **113**, 155004 (2014).